Strain broadening of the magnetization steps in diluted magnetic semiconductors

Yuri G. Rubo* and M. F. Thorpe†
Department of Physics and Astronomy, Michigan State University, East Lansing, Michigan 48824-1116

Normand Mousseau‡
Département de Physique, Université de Montréal, Case Postale 6128, Montréal, H3C 3J7, Canada
(Received 13 May 1997)

We show that the bond-length mismatch in magnetic solid alloys (diluted magnetic semiconductors) results in fluctuations of the exchange constants between neighboring magnetic ions. We present the theory of these fluctuations and analyze their effect on the broadening of magnetization steps observed in these materials. We conclude that the effect is quantitatively comparable to the effect of the Dzyaloshinski-Moriya interaction, but produces a different behavior of the magnetization curve, which gives a possibility to distinguish between these mechanisms experimentally. [S0163-1829(97)07544-9]

I. INTRODUCTION

Peculiarities in the structure of random semiconductor solid alloys, which can be represented by the general formula $A_{1-x}B_xC$ (e.g., for the case of a ternary alloy like $Ga_{1-x}In_xAs$ or $Cd_{1-x}Mn_xTe$), are mainly related to the existence of the difference between natural bond lengths and force constants for the A-C and B-C bonds. Placed randomly in the alloy the A and B atoms try to achieve their natural covalent radii, producing random compressions and expansions across the alloy. It is important to note that the length of a given bond depends not only on its local environment but also on the distribution of atoms in some macroscopic surrounding volume, because of the long-range character of elastic forces.

Experimentally the mean A-C and B-C bond lengths of the alloy and their rms fluctuations are studied using the technique of extended x-ray absorption fine structure (XAFS) measurements.[1–3] It has been found that the average cation-anion distance in the ternary alloy and, correspondingly, the average lattice constant, obey Végard's law,[4] i.e., they vary linearly with composition x. At the same time the alloy exhibits a pronounced bimodal structure: where the average A-C and B-C bond lengths remain close to their values in the corresponding binary prefect crystals and vary only a little (also practically linearly) with the composition x. The linear dependencies of mean distances between neighbors in the lattice on the composition suggest that the *force constant* disorder plays a rather insignificant role and that the *bond length* disorder is dominant. Neglecting the force constant disorder allows the possibility to elaborate the theory of the alloy structure in a general analytic form.[5,6] It has been shown that the structure can be completely described by a set of topological rigidity constants that are defined by the geometry of underlying lattice. These constants were calculated in Ref. 6 for the zinc-blende lattice using the framework of the Kirkwood and Keating models.[7,8]

In this paper we discuss the possible effects of the structural disorder in magnetic semiconducting alloys, the so-called semimagnetic semiconductors or diluted magnetic semiconductors (DMS's), on their magnetic properties. DMS's are solid alloys belonging to the family of II-VI semiconductors, where some fraction of the cations are substituted with transition magnetic ions from the iron group, like $Cd_{1-x}Mn_xTe$.[9] The magnetic properties of DMS's are mainly attributed to the existence of an antiferromagnetic (AF) exchange interaction between the magnetic ions, and the physical nature of this interaction is now well established to be superexchange.[10–12] It has been found[10,13] that the AF exchange constant rapidly decreases with the distance between the two ions in the lattice, so that the most important interaction is between the ions which are nearest neighbors (NN's). The superexchange mechanism for NN interactions predicts the strong dependence of the exchange constant on both the the *angle* formed by the bonds connecting these ions with the neighboring anion and on the *lengths* of these bonds. In particular, the mean Mn-Te-Mn angle is slightly different for different zinc-blende DMS compounds [and differs also from the perfect tetrahedral value $\cos^{-1}(-1/3)$]. The mean angle *increases* when one goes from $Zn_{1-x}Mn_xTe$ to $Hg_{1-x}Mn_xTe$ and then to $Cd_{1-x}Mn_xTe$, and this leads to a *decrease* in the value of the Mn-Mn exchange constant.[12] So, one could expect from these results that the disorder in the distribution of magnetic ions over the lattice sites and fluctuations in the geometry of different NN pairs of magnetic ions in the alloy should produce fluctuations of the *exchange constant* for different pairs of ions in a given DMS. Experimentally, this nearest-neighbor exchange seems to follow closely the Mn-Mn distance (independently of the ligand) as shown in Fig. 1, and we will use this simple and perhaps surprising result in this paper.

The physical phenomenon in DMS's, which is sensitive to the above-mentioned fluctuations of the NN exchange constant and which is under detailed consideration in this paper, is the magnetization steps observed in the magnetization curve of DMS's in high magnetic fields (see, Ref. 14 and references therein). These steps appear because of the antiferromagnetic nature of the exchange interaction between the ions. In this case the NN pairs of Mn ions possess zero spin in low magnetic fields and do not contribute to the magnetization of the alloy. As a result, the magnetization in low and moderate fields is mainly due to single ions, and it follows

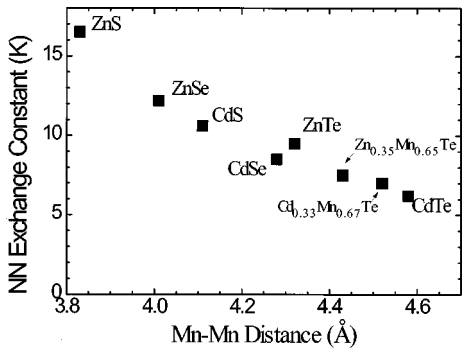

FIG. 1. Showing the dependence of the nearest-neighbor exchange constant J_1 between Mn-Mn pairs for different DMS compounds. All the compounds shown are in the very dilute Mn concentration limit, except for the two samples marked. The dependence is adequately described by a straight line with a slope of -14 K/Å. This figure is from J. K. Furdyna (private communication) and based on data of Furdyna.

that a Curie law is expected with an apparent saturation in the region where single ions become completely polarized. Additional increase of the magnetic field, however, breaks down the antiferromagnetic alignment of ions in a pair and the pairs begin to contribute to the magnetization. The change of the spin of each pair is quantized and is caused by the change in the nature of the ground state of the pair in a magnetic field. When the magnetic field reaches the critical value $2J_1/(g\mu_B)$, where J_1 is the absolute value of the NN exchange constant, $g\approx 2$ is the g factor of Mn, and μ_B is the Bohr magneton, the state of the pair with total spin $S=1$ and its projection $\mu=-1$ crosses the state with $S=0$ and becomes the ground state. At this point the first step arises in the magnetization curve. Then, at a field $4J_1/(g\mu_B)$ the state with $S=2$, $\mu=-2$ becomes the ground state and the second step appears, and so on. Since the Mn^{++} ion possesses a 5/2 spin, a total of five steps due to NN pairs can be observed.[15] Experimentally observed steps are not sharp and their positions B_{cn} are shifted a little from those given above. This shift in the positions is due to the exchange interaction of the NN pairs with more distant Mn ions, in particular, with the next nearest neighbors of the ions belonging to the pair.[16] For the broadening of the magnetization steps, several mechanisms have been discussed up to date. First is the simple thermal broadening. The second reason for an increasing of the step width[17] is the Dzyaloshinski-Moriya (DM) interaction, which is present for two ions in a pair along with the dominant Heisenberg interaction.[18,11,19] Then, the interaction of ions in a pair with distant neighbors not only shifts the positions of the step but also affects the step shape.[16] We show in this paper that there exists one additional mechanism for the step broadening. Namely, the above-mentioned fluctuations of Mn-Mn distance, and, correspondingly, the NN exchange constant, produce fluctuations in the positions of the crossing points B_{cn} $(n=1,2,3,4,5)$, i.e., they result in an inhomogeneous broadening of the steps. It turns out that each of these mechanisms leads to different shapes of the steps and, what is most important, they possess substantially different dependences on the step number, which gives the possibility to independently access the relative importance of each mechanism from the experimental data.

The paper is organized in the following way. The theory of strain fluctuations of NN pairs in a ternary alloy is developed in Sec. II below. Sec. III is devoted to the analysis of the mechanisms of additional broadening of the magnetization steps: interaction with distant neighbors, DM interaction between the ions in the pair, and strain-induced broadening. Finally, Sec. IV contains a discussion of the results and conclusions.

II. STRAIN EFFECTS

We consider a ternary alloy $A_{1-x}B_xC$ that in the absence of the bond-length mismatch for the A-C and B-C bonds would form a perfect zinc-blende lattice. The sites of this perfect lattice are given by vectors **i** (for the sublattice containing A and B atoms; in what follows, this sublattice will be referred as the cation sublattice) and **j** (for the anion sublattice which contains C atoms only). The bond-length mismatch is usually small for known semiconductor solid alloys, i.e., the difference of natural bond lengths $L^0_{AC}=\rho^0_A+\rho^0_C$ and $L^0_{BC}=\rho^0_B+\rho^0_C$ (where ρ^0_A denotes the covalent radius of the A atom, etc.) is small compared to the mean cation-anion bond length in the alloy $L_e=(1-x)L^0_{AC}+xL^0_{BC}$. In this case, the typical displacements $\{\mathbf{u_n}\}$ of the atoms from their positions in the perfect lattice are also small, and the strain-induced energy $V(\{\mathbf{u_n}\})$ can be written as a quadratic form with respect to the displacements. Then, the equilibrium positions of the atoms are the same as in the case when there would be a perfect crystal with random forces applied to the atoms. With interactions of nearest anion-cation neighbors only, the force on an anion can be written as

$$\mathbf{F_j}=-\alpha\sum_{\mathbf{i(j)}}\rho^0_{\mathbf{i}}\hat{\mathbf{r}}_{\mathbf{ji}}, \tag{1}$$

where the notation **i**(**j**) means the summation over the four nearest-neighboring cation sites of the **j**th anion site, $\hat{\mathbf{r}}_{\mathbf{mn}}$ is the unit vector from site **m** to site **n** of the underlying perfect lattice, and α is a spring constant of the bond (it is assumed to be the same for A-C and B-C bonds). Note that random forces are applied to the anions only; the force on a cation $\mathbf{F_i}=0$, because of there is no disorder in the anion sublattice.

The problem of finding out the displacements $\{\mathbf{u_n}\}$ is thus reduced to the solution of the system of linear equations $\Sigma_{\mathbf{m}}\mathbf{D_{nm}}\cdot\mathbf{u_m}=\mathbf{F_n}$, where $\mathbf{D_{nm}}$ is the dynamical matrix of the crystal. It is perhaps surprising, but correct, that the dynamical matrix $\mathbf{D_{nm}}$ has the full translational symmetry of the perfect virtual crystal. This is because force constant disorder has been neglected.

Inverting this equation we have

$$\mathbf{u_n}=\sum_{\mathbf{m}}\mathbf{G_{nm}}\cdot\mathbf{F_m}, \tag{2}$$

with $\mathbf{G_{nm}}$ being the phonon Green function. Substituting Eq. (1) into Eq. (2) we can write down the deviation of the distance between an arbitrary pair of sites, say **n** and **m**, from its value in the perfect lattice $L^e_{\mathbf{nm}}$ (cf. Ref. 6):

$$L_{\mathbf{nm}}-L^{e}_{\mathbf{nm}}=\hat{\mathbf{r}}_{\mathbf{nm}}\cdot(\mathbf{u}_{\mathbf{m}}-\mathbf{u}_{\mathbf{n}})=\sum_{\mathbf{i}} a_{\mathbf{nm,i}}\rho^{0}_{\mathbf{i}}, \tag{3}$$

$$a_{\mathbf{nm,i}}=\alpha\sum_{\mathbf{j(i)}} \hat{\mathbf{r}}_{\mathbf{nm}}\cdot(\mathbf{G}_{\mathbf{nj}}-\mathbf{G}_{\mathbf{mj}})\cdot\hat{\mathbf{r}}_{\mathbf{ji}}. \tag{4}$$

Disorder enters the expression (3) only through the cation covalent radius $\rho^{0}_{\mathbf{i}}$, which takes the value ρ^{0}_{A} if site $\mathbf{i}$ is occupied by an A atom, and the value ρ^{0}_{B} otherwise. The dimensionless three-point function $a_{\mathbf{nm,i}}$ can be calculated, in principle, using a given model for the phonon spectrum of the crystal. It is seen from the definition (4) that $a_{\mathbf{nm,i}}=a_{\mathbf{mn,i}}$. It also follows from the translational symmetry that $a_{\mathbf{nm,i}}$ depends only on differences $\mathbf{i}-\mathbf{n}$ and $\mathbf{i}-\mathbf{m}$ and obeys the condition

$$\sum_{\mathbf{i}} a_{\mathbf{nm,i}}=0. \tag{5}$$

A. Conditional averaging

Equation (3) makes it possible to find general expressions for the mean distance and its rms fluctuation for any two atoms in the alloy.[6] The expressions obtained in Ref. 6, however, cannot be applied directly to the analysis of the geometry of NN pairs. In particular, in calculating the mean distance between two B atoms which form a pair, we should *exclude* situations when either one of these atoms has another nearest-neighbor B atom, because then this would not be an isolated pair, but part of a larger cluster. In other words, we have to perform averaging with the *condition* that this pair of B atoms is surrounded by A atoms only.

A generic statement of such a problem is as follows. Let us assume that there is a well-defined distribution of A and B atoms in some part of the alloy. The A atoms of interest occupy a subset of cation sites $\mathcal{V}_A$ and B atoms of interest occupy a subset $\mathcal{V}_B$. Superposition of $\mathcal{V}_A$ and $\mathcal{V}_B$ defines a cluster $\mathcal{V}$. In particular, in the case of an isolated pair of B atoms, $\mathcal{V}_B$ consists simply of two nearest-neighboring sites in the cation sublattice and $\mathcal{V}_A$ could be cation sites in the first nearest-neighbor shell around this pair (see Fig. 2). All other sites of the lattice are occupied at random by B atoms with probability x and by A atoms with probability $(1-x)$. Then, performing the averaging of Eq. (3) for sites outside of the cluster and making use of the summation rule (5), we obtain the following expression for the mean distance between two arbitrary sites $\mathbf{n}$ and $\mathbf{m}$ belonging to cluster $\mathcal{V}$:

$$\langle L^{(\mathcal{V})}_{\mathbf{nm}}\rangle=L^{e}_{\mathbf{nm}}+(\rho^{0}_{A}-\rho^{0}_{B})[x\mathcal{G}^{\mathbf{nm}}_{A}-(1-x)\mathcal{G}^{\mathbf{nm}}_{B}], \tag{6}$$

$$\mathcal{G}^{\mathbf{nm}}_{A}=\sum_{\mathbf{i}\in\mathcal{V}_A} a_{\mathbf{nm,i}}, \quad \mathcal{G}^{\mathbf{nm}}_{B}=\sum_{\mathbf{i}\in\mathcal{V}_B} a_{\mathbf{nm,i}}, \tag{7}$$

where $L^{e}_{\mathbf{nm}}$ is again the distance between these sites in the virtual lattice given by mean lattice constant $L_e=(1-x)\rho^{0}_{A}+x\rho^{0}_{B}+\rho^{0}_{C}$ multiplied by the appropriate geometrical scale factor. The fluctuation of the $L^{(\mathcal{V})}_{\mathbf{nm}}$ also can be found from Eq. (3) to be

$$\langle(L^{(\mathcal{V})}_{\mathbf{nm}}-\langle L^{(\mathcal{V})}_{\mathbf{nm}}\rangle)^2\rangle=x(1-x)(\rho^{0}_{A}-\rho^{0}_{B})^2\mathcal{R}^{\mathbf{nm}}_{\mathcal{V}}, \tag{8}$$

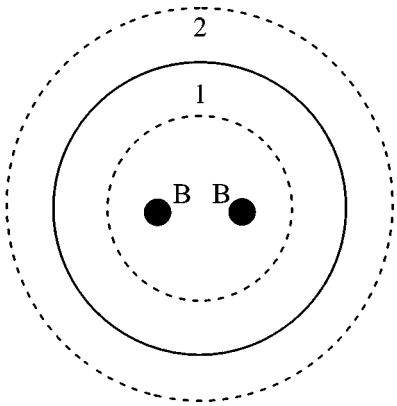

FIG. 2. Schematic representation of the isolated pair of B atoms in $A_{1-x}B_xC$ alloy. The $\mathcal{V}_B$ cluster discussed in the text is just these two sites of the cation sublattice. For the pair to be isolated it is necessary that all NN cation sites for these two (shell 1) are occupied by the A atoms. The eighteen cation sites in the shell 1 will then form the $\mathcal{V}_A$ cluster. The second shell contains further 51 additional A sites.

$$\mathcal{R}^{\mathbf{nm}}_{\mathcal{V}}=\sum_{\mathbf{i}\notin\mathcal{V}} a^{2}_{\mathbf{nm,i}}. \tag{9}$$

The lattice integrals (7),(9) determining the average deformation of the lattice are independent of the concentration of impurities as well as the size mismatch *per se*, and they represent a fundamental property of the lattice. This comes about because the alloy is considered as a perfect solid solution from which some particular clusters $\mathcal{V}$ are selected for averaging. Any correlation between the atomic species would destroy the universality of the lattice integrals and introduce a dependence on size mismatch and atomic concentrations into these integrals. However, II-VI pseudobinaries, can be considered as good examples of solid solutions and should be well described by the above equations.

In the case shown in Fig. 2, the isolated pair of B atoms, two properties of the lattice integrals (7),(9) are worth mentioning, which concerns their behavior with increasing of the size of the $\mathcal{V}_A$ cluster. If we denote by $\mathcal{G}_{nA}$ the lattice integral for the case of a pair isolated from other A atoms inside all the shells up to the nth shell, the sum rule (5) implies that $\mathcal{G}_{nA}$ will approach $-\mathcal{G}_B$ when n goes to infinity. If we denote by $\mathcal{R}_{n\mathcal{V}}$ the lattice integral for the fluctuations in a similar way, then we show in the Appendix that $\mathcal{R}_{n\mathcal{V}}$ will go to zero as a power of the nth shell radius $|\mathbf{R}_n|$, namely, as $|\mathbf{R}_n|^{-3}$ for the 3D lattice.

B. Numerical simulations

In general, it is quite difficult to perform the lattice integrals on the phonon Green's functions as given by Eqs. (4), (7), and (9). This is because in calculating of the tensor $\mathbf{G}_{\mathbf{nm}}$ one encounters integrals over the Brilloin zone with an oscillating integrand. To illustrate this point we present the solution for the 2D triangular lattice in the Appendix. For the 3D zinc-blende lattice, however, an analytical integration is not feasible and we are left with two possible approaches: a numerical integration or a direct measurement either from experimental data or numerical simulations. The latter ap-

proach is much preferable since a single simulation is sufficient for extracting all the Green's-function integrals. We simply minimize the configurational energy of the given realization of a solid solution and then obtain the integral values by inverting Eqs. (6) and (8). As the integrals themselves are independent of concentration and size mismatch, the validity of these equations can also be confirmed by varying these parameters.

Simulations are performed on unit cells of $8\times(64)^2=32\,768$ atoms with periodic boundary conditions. Atoms are first distributed at random on a zinc-blende lattice, as appropriate to the concentration x. The atomic positions are then relaxed with an energy minimization conjugate-gradient algorithm.[20] The setup is identical to previous work:[5] a Kirkwood potential is used and the alloy on the first sublattice is considered to be a perfect solid solution. The Kirkwood potential consists of separate two- and three-site harmonic interactions:

$$E=\frac{\alpha}{2}\sum_{\langle ij\rangle}(L_{ij}-L_{ij}^{0})^2+\frac{\beta}{8}L_e^2\sum_{\langle ijl\rangle}(\cos\theta_{ijl}+\tfrac{1}{3})^2, \quad (10)$$

where α is the same as in Eq. (1) and β is an angular force constant. Values for the lattice integrals are functions of the topology of the lattice as well as of the ratio β/α, which determines the importance of angular forces versus the central forces. Our results are sensitive only to the ratio β/α, and not to the absolute value of α. In II-VI semiconductor compounds, this ratio is normally around $\beta/\alpha=0.10$ (Ref. 5) and can go up to about 0.20 in III-V and IV-IV materials.[5,22] Although elastic constants vary with atomic species, they typically differ by at most 20%. As was shown previously, such small variations do not produce changes that are significant or detectable when measuring structural properties.[5]

We are interested here in isolated atomic pairs (the B atoms). It is therefore necessary to work at relatively low concentrations x so as to decrease the statistical weight of large clusters. The total concentration of B-B pairs (which we will refer to as $P0$) on the lattice without any restriction on their environment is $6x^2$. The total concentration of B-B pairs, with no B atoms in the first-neighbor surrounding shell ($P1$) goes as $6x^2(1-x)$[18], while that for B-B pairs with no B atoms in either the first- or second-neighbor surrounding shell ($P2$) is $6x^2(1-x)^{69}$ (cf. Ref. 21). The maximum for $P1$ is at $x=0.10$ and that for $P2$ is around $x=0.03$. Note that at $x=0.05$ there are only six or seven $P2$ pairs in the 32 768 atom cell.

To improve statistics, five realizations of disorder are averaged for each value of the concentration x and the force constant ratio β/α. For numerical efficiency, we select a size mismatch much larger than for real materials: the conjugate-gradient algorithm limits the precision on the total energy to about 1 part in 10^{10}; given the size of our unit cells, it is important to enhance the cost of disorder as much as possible to obtain a good relaxation. Since the magnitude of the size mismatch does not enter in the lattice integrals, this numerical trick does not affect the final solution as was also confirmed by comparing results for different size mismatches. The final results discussed here were obtained for a size mismatch of 9.7%—about four times larger than for $Cd_{1-x}Mn_xTe$, which reduces by more than half the number of conjugate-gradient (CG) steps needed to achieve full convergence.

TABLE I. The lattice integrals involved in the calculation of the average Mn-Te and Mn-Mn mean distances. The data are obtained following the prescription given in the text, and are for exclusion zones around the magnetic pair of interest as described in the text.

	β/α 0.05	0.10	0.15
Mn-Te			
$\mathcal{G}_{0A}$	0.00	0.00	0.00
$\mathcal{G}_{1A}$	-0.09 ± 0.01	-0.12 ± 0.02	-0.13 ± 0.01
$\mathcal{G}_{2A}$	-0.10 ± 0.02	-0.12 ± 0.05	-0.10 ± 0.02
$\mathcal{G}_{B}$	0.84 ± 0.01	0.74 ± 0.01	0.67 ± 0.01
Mn-Mn			
$\mathcal{G}_{0A}$	0.00	0.00	0.00
$\mathcal{G}_{1A}$	-0.15 ± 0.15	-0.16 ± 0.04	-0.14 ± 0.04
$\mathcal{G}_{2A}$	-0.43 ± 0.30	-0.42 ± 0.22	0.02 ± 0.20
$\mathcal{G}_{B}$	0.65 ± 0.02	0.56 ± 0.02	0.48 ± 0.01

For the pairs of interest in this paper, the quantity $\mathcal{G}_B^{\mathbf{nm}}=\mathcal{G}_B$ is independent of the size of the exclusion zone for other B atoms around the pair, and is the same as the unconditional average. The quantity $\mathcal{G}_B$ is shown in Table I for the case where n,m are nearest-neighbor Mn-Te pairs and when n,m are next-nearest-neighbor Mn-Mn pairs (i.e., nearest-neighbor magnetic pairs). For the nearest-neighbor Mn-Te and Mn-Mn distances, the lattice integral $\mathcal{G}_B$ is the same for all such pairs and is equivalent to $a_{BC}^{**}(111)$ and $a_{BB}^{**}(220)$ of Ref. 6. The notation for n,m is the same as described above, and $\mathcal{G}_{0A}$, $\mathcal{G}_{1A}$, and $\mathcal{G}_{2A}$ refer to no exclusion zone, one-shell exclusion and two-shell exclusion, respectively. When there is no restriction on the environment of these pairs, Eqs. (6) and (8) become identical to Eq. (20) of Ref. 6 and $\mathcal{R}_0\equiv b_{BB,C}^{**}$.

Tables I and II give the numerical values for the lattice integrals (7) and (9) at three force constants ratios. As predicted by the theory and verified numerically, these values are independent of the concentration and size mismatch. Errors are estimated from the spread of values for different realizations of disorder.

TABLE II. The lattice integrals that determine the rms fluctuations in the Mn-Mn pair distance. These values are extracted from numerical simulation invoking Eq. (8) following the procedure described in the text, and for various sizes of the exclusion zone around the magnetic pair of interest.

	β/α 0.05	0.10	0.15
Mn-Te			
$\mathcal{R}_0$	0.0050 ± 0.0010	0.0130 ± 0.0010	0.0180 ± 0.0040
$\mathcal{R}_1$	0.0011 ± 0.0001	0.0023 ± 0.0003	0.0031 ± 0.0004
$\mathcal{R}_2$	0.0003 ± 0.0001	0.0005 ± 0.0004	0.0007 ± 0.0003
Mn-Mn			
$\mathcal{R}_0$	$0.560\ \pm0.087$	$0.421\ \pm0.025$	$0.283\ \pm0.068$
$\mathcal{R}_1$	$0.101\ \pm0.011$	$0.066\ \pm0.008$	$0.044\ \pm0.012$
$\mathcal{R}_2$	$0.019\ \pm0.010$	$0.019\ \pm0.012$	$0.010\ \pm0.003$

III. MAGNETIZATION STEPS

Now we consider the broadening of the steps arising on the magnetization curve of the DMS from the pairs of magnetic ions. The Hamiltonian of an isolated pair of Mn ions (possessing spins $\mathbf{S}_1$ and $\mathbf{S}_2$ with $S_1=S_2=5/2$) in a magnetic field B applied along the $\hat{z}$ direction reads

$$H_p=2J(\mathbf{S}_1\cdot\mathbf{S}_2)+g\mu_B(B-b)(S_{1z}+S_{2z})+H_{\mathrm{DM}}, \quad (11)$$

$$H_{\mathrm{DM}}=2\mathbf{D}\cdot(\mathbf{S}_1\times\mathbf{S}_2). \quad (12)$$

Here $b>0$ describes the antiferromagnetic exchange interaction of a given pair with distant neighbors[16] and H_{DM} is the Dzyaloshinski-Moriya interaction between the ions.[18] The axial vector $\mathbf{D}$ in Eq. (12) is perpendicular to the plane containing these two Mn ions and the adjacent anion, and, since the DM interaction is a relativistic effect, $|\mathbf{D}|\ll J$.

The contribution of a given pair to the magnetization of the sample is proportional to its average spin,

$$m=-\frac{\mathrm{Tr}\{(S_{1z}+S_{2z})\exp(-H_p/kT)\}}{\mathrm{Tr}\{\exp(-H_p/kT)\}} \quad (13)$$

[a minus sign is introduced in Eq. (13) for convenience, so that $m>0$]. The behavior of m as a function of applied magnetic field at low temperature ($kT\ll J$) is steplike:[14] m is close to zero for small fields, then changes sharply to 1, then to 2, and so on, until it reaches its maximum value of 5. The appearance of these steps corresponds to the change of the spin of the ground state of the Hamiltonian (11).

If one neglects the DM term (12), the eigenstates $|S,\mu\rangle$ of H_p can be classified by values of the total spin of the pair $S=0,1,2,3,4,5$, and the $\hat{z}$-component μ of the pair. The positions of the steps $B_n(b)$ can be found then from the condition of crossing of the $|S,-S\rangle$ and $|S+1,-(S+1)\rangle$ energy levels. For the nth step one has[16,14]

$$B_n(b)=n(2J/g\mu_B)+b, \quad n=1,2,3,4,5. \quad (14)$$

The shape of each step in the dependence $m(B)$ for a given pair with $H_{\mathrm{DM}}=0$ has thus a pure thermal nature and is given by a Fermi-distribution-like function, which reflects the relative probabilities for the pair to be found in states $|S,-S\rangle$ and $|S+1,-(S+1)\rangle$ near the crossing point. This thermal broadening is the same for all steps because the energy difference $E(S+1,-(S+1))-E(S,-S)=2J-g\mu_BB$ does not depend on $S=n-1$.

Instead of analyzing the function $m(B)$ it is more convenient to deal with its derivative, dm/dB, which exhibits five peaks as a function of the applied magnetic field B. In the case when the separation between adjacent peaks $2J/g\mu_B$ is much greater than the peak width one can discuss each peak separately. In particular, the thermal width of the nth peak can be characterized by the average value of $(B-B_n(b))^2$,[14]

$$\int (B-B_n(b))^2\frac{dm}{dB}dB\equiv\frac{\Delta_T^2}{(g\mu_B)^2}=\frac{\pi^2}{3}\left(\frac{kT}{g\mu_B}\right)^2, \quad (15)$$

where the main contribution to the integral is from an interval $2J/g\mu_B$ around B_n and we assumed $\Delta_T\ll J$. The experimentally observed magnetization is the result of superposition of $m(B)$ from different pairs in the sample, and different pairs possess slightly different exchange constants, as was discussed in Sec. I, and are subject to different local exchange fields b. The average value of $m(B)$,

$$M(B)=\langle m(B)\rangle, \quad (16)$$

with respect to fluctuations in J and b exhibits steps with an additional broadening. We will analyze these three effects in detail in subsections that follow.

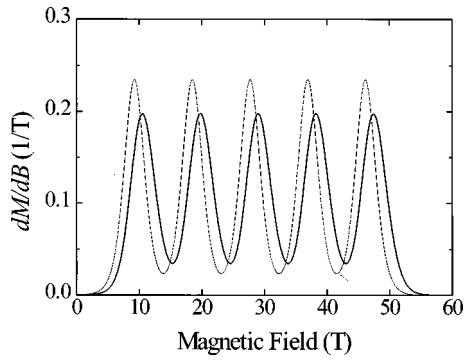

FIG. 3. Showing the shift and small additional broadening of peaks in the derivative dM/dB of the average spin of Mn-Mn pair in $Cd_{0.95}Mn_{0.05}Te$ (exchange constant $J_1=6.2$ K) when the internal exchange field from distant neighbors is taken into account (solid line). The dashed line shows the pure thermal broadening at $T=1.4$ K. The exchange constants describing the coupling to distant neighbors are $J_2=0.6$ K, $J_3=0.3$ K.

A. Interaction with distant neighbors

The theory of internal exchange field acting on Mn-Mn pairs in DMS was developed in Ref. 16. In this subsection we use the results[16] and calculate the average spin (16) of the Mn-Mn pair primarily to show the qualitative differences between this effect, DM and strain broadening mechanisms, and for the sake of completeness.

The internal exchange field b entering the pair Hamiltonian (11) arises due to the interaction between Mn ions in the pair under consideration and Mn ions occupying second, third, etc. cation shells around these two ions. Because the Mn-Mn exchange interaction decreases rapidly with the distance,[10,13] it is sufficient to take into account the antiferromagnetic exchange with Mn ions in the second shell (absolute value of exchange constant is J_2) and with Mn ions in the third shell (absolute value of exchange constant is J_3) only.[16] In this case b takes on a set of discrete values (which are linear combinations of J_2 and J_3) with probabilities being dependent on the concentration of the alloy x. Using this distribution function of internal field b given by Table II of Ref. 16 we have convoluted the average spin of the Mn-Mn pair (13) and the result is shown on Fig. 3. For the calculation we have chosen DMS $Cd_{1-x}Mn_xTe$ with the smallest NN exchange constant [$J\equiv J_1=6.2$ K (Ref. 15)] and with a concentration of Mn ions $x=0.05$, which is the typical concentration for the magnetization steps measurements (the relative contribution of pairs to the magnetization of the sample has its maximum at this point[14]). The NNN exchange constants were taken according to the approximate relations $J_2\simeq J_1/10$ (Refs. 23 and 24) and $J_3\simeq J_2/2$.[13]

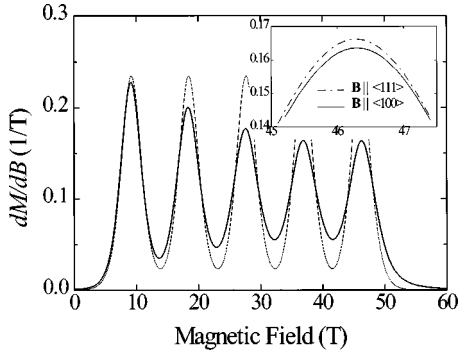

FIG. 4. The derivative of the average spin of Mn-Mn pairs in $Cd_{1-x}Mn_xTe$ (exchange constant $J_1=6.2$ K) in the presence of the DM interaction (12). The results were obtained for $|\mathbf{D}|=0.3\ \mathrm{K}\simeq 0.05J_1$ (Refs. 11 and 18). The dashed line shows the pure thermal broadening ($D=0$) at $T=1.4$ K. The difference between the average spin of the pairs for two different orientations of the applied magnetic field is shown in the inset (see the text).

It follows from Fig. 3 that the interaction with distant neighbors results mainly in the shift of the position of the peaks, but only slightly affects the peak width (as is seen from the change in the peak amplitudes). The value of the shift, $B_{cn}-(2J/g\mu_B)=0.91J_2+4.56J_3$ at $x=0.05$,[16] is independent of the peak number. The (small) change in the peak width arising due to this mechanism is also the same for all five peaks and can be described by introducing an effective temperature T^*, so that at $x=0.05$

$$(kT^*)^2=(kT)^2+\frac{3}{\pi^2}(2.10J_2^2+1.33J_2J_3+10.95J_3^2). \tag{17}$$

B. DM interaction

In spite of the fact that it is generally accepted that the DM interaction (12) produces additional broadening of the magnetization steps,[14] we did not find a detailed analysis of this effect in the literature. That is why in this subsection we present the theory of the shape of the magnetization steps in the presence of DM interaction.

It is clear from Eqs. (11) and (12) that the energy spectrum of a given pair depends on the angle ϕ between the applied magnetic field **B** and the vector **D**. Because Mn-Mn pairs are placed in a zinc-blende lattice, there are six possible directions of the DM vector **D**: $\langle 110\rangle$, $\langle 101\rangle$, $\langle 011\rangle$, $\langle \bar{1}10\rangle$, $\langle \bar{1}01\rangle$, and $\langle 0\bar{1}1\rangle$. The spin of Mn-Mn pair (13) should thus be averaged over the different directions of **D**, and the result of such averaging will, in general, depend on the direction of magnetic field. Indeed, in the case $\mathbf{B}\|\langle 100\rangle$ one has $\cos(\phi)=0$ for 25% of pairs, and $\cos(\phi)=\pm 1/\sqrt{2}$ for 75% of pairs; in the case $\mathbf{B}\|\langle 111\rangle$ already 50% of pairs have $\cos(\phi)=0$, and $\cos(\phi)=\sqrt{2/3}$ for the other 50%.

In Fig. 4 we show the dependence of the averaged (as explained above) derivative of the magnetization on the applied magnetic field. The results were obtained by numerical diagonalization of the Hamiltonian (11),(12), which is a 36×36 matrix. The internal exchange field b was omitted for simplicity. It turned out that the anisotropy is quite small, as is seen from the inset showing the maximum of the fifth peak (where the anisotropy is the strongest). The anisotropy becomes bigger with decreasing temperature, but the difference between the maximum value at the fifth peak for $\mathbf{B}\|\langle 100\rangle$ and $\mathbf{B}\|\langle 111\rangle$ is only a few percent at $T=0.2$ K.

Because the results in Fig. 4 correspond to $T=1.4$ K, the DM interaction affects only slightly the width of the peaks. It does affect noticeably, however, their *amplitudes*. And most remarkable in Fig. 4 is the fact that the effect depends on the number of the peak, contrary to the case of the broadening due to interaction with distant neighbors. The dependence on the peak number is not monotonic: the change in the amplitude is tiny for the first peak, it increases rapidly from the second to the fourth peak, but the effect on the last, fifth peak is approximately the same as on the fourth peak, or even a little bit smaller.

To understand this behavior we note that the DM interaction leads to an additional broadening of the magnetization steps because it mixes the $|S,-S\rangle$ and $|S+1,-(S+1)\rangle$ states of the pair near the crossing point, resulting in an avoided crossing.[14] The value of this effect is related to the matrix element of H_{DM} between these two states. It is seen from Eq. (12) that one has to calculate the following numbers:

$$d_{S+1}=|\langle S+1,-(S+1)|(\mathbf{S}_1\times\mathbf{S}_2)_-|S,-S\rangle|^2, \tag{18}$$

which can be written via the Clebsch-Gordan coefficients. The calculations show that d_n, which defines the additional broadening of nth peak, is indeed a nonmonotonous function of n, explaining the behavior of dM/dB in Fig. 4. Namely, $d_1=35/6=5.8$, $d_2=128/5=25.6$, $d_3=729/14=52.1$, $d_4=640/9=71.1$, and $d_5=125/2=62.5$. Note that coefficients increase at the beginning, but d_5 is *smaller* than d_4, and this makes the height of the last peak slightly greater then the amplitude of the fourth one.

The second moment of the peaks in dM/dB is infinite because of a logarithmic divergence associated with the tails, in the limit when the peaks are well separated as happens with a small D at low temperature. Thus it is not possible to define an effective temperature as was done at the end of the previous section. The full width at half the peak height scales as D of course.

C. Strain broadening

Now we come back to consideration of the fluctuations in the geometry of Mn-Mn pairs and the inhomogeneous broadening of the magnetization steps due to related fluctuations in Mn-Mn exchange constant J. First of all, it worth noting from Table II that fluctuations of Mn-Te distances in the alloy are about an order of magnitude smaller than the fluctuations of Mn-Mn distances. This is a consequence of the strong inequality between radial and angular forces: $\alpha\gg\beta$. The problem of finding the fluctuations in the exchange constant is thus reduced to analyzing the one parameter dependence of $J(L)$, where L is Mn-Mn separation.

Detailed information about the dependence $J(L)$ was obtained by means of inelastic neutron scattering from II-VI diluted magnetic semiconductors,[25] as well as from the positions of the magnetization steps. It was discovered that if one takes the values of J for NN Mn-Mn pairs in different DMS's and plot them as a function of *mean* Mn-Mn distance

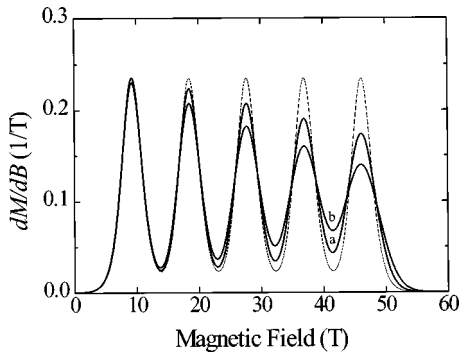

FIG. 5. Showing the effect of fluctuations in the Mn-Mn exchange constant J in $Cd_{1-x}Mn_xTe$ on the dM/dB curve (see explanations in the text). The dashed line is the same as in Figs. 1 and 2, and shows the pure thermal broadening at $T=1.4$ K. The mean value of the exchange constant is $\langle J\rangle \equiv J_1 = 6.2$ K. Solid curves in this figure correspond to root-mean-square fluctuations of the exchange constant, δJ, equal to $\delta J = 0.2$ K (a) and $\delta J = 0.3$ K (b).

in corresponding materials, the points fall on a very good straight line,[25] as shown in Fig. 1. From the slope of this line one can find that $dJ/dL \simeq -14$ K/Å. Note also that the dependence $J(L)$ defines the interaction between the spin of Mn ions in a pair and the phonons in the system. The value $|J/(dJ/dL)| = 0.35$ Å was used in Ref. 26 when analyzing the spin relaxation, which leads to somewhat higher derivative, $dJ/dL \simeq -18$ K/Å for $Cd_{1-x}Mn_xTe$. From these data and using Eq. (8) and Table II, we can find out the typical rms fluctuation of the NN Mn-Mn exchange constant in $Cd_{0.95}Mn_{0.05}Te$ to be about 0.2 K [the values of covalent radii entering Eq. (8) were taken as $\rho^0_{Cd} = 1.48$ Å and $\rho^0_{Mn} = 1.30$ Å (Refs. 27–29)].

The strain-induced broadening of magnetization steps is shown in Fig. 5. In calculating dM/dB we have convoluted the average spin of the Mn-Mn pair (13) with a Gaussian distribution of exchange constants. This was done having in mind that the distribution of cation-cation distances is close to Gaussian[5] and J and L are linearly related. It is seen from Fig. 5 that the case of strain broadening is similar to the Dzyaloshinski-Moriya one: the main effect is on the peak amplitudes, but the behavior of the amplitude as a function of the peak number n is *monotonic*. The fact that the peak amplitude decreases linearly with n can be understood if one recalls that the position of nth peak is found from the relation $B_n = n(2J/g\mu_B)$ [i.e., from Eq. (14) in which we neglected the internal exchange field b.] So, for a given fluctuation in the exchange constant, the corresponding fluctuations in the positions of peaks, and thus the additional inhomogeneous broadening of peaks, increase linearly in n. In the case of low temperatures, when the peaks are well separated, one can also define some effective temperature to describe the strain broadening of the nth peak:

$$(kT_n^*)^2 = (kT)^2 + \frac{12}{\pi^2}(n\,\delta J)^2, \tag{19}$$

where δJ is the rms fluctuation of J.

IV. DISCUSSION AND CONCLUSIONS

Comparing Figs. 3–5 we can point out that the three mechanisms of additional (with respect to the pure thermal) broadening of the magnetization steps in DMS, namely, (i) interaction of Mn-Mn pair with distant neighbors, (ii) the Dzyaloshinski-Moriya interaction between the ions in the pair, and (iii) the strain induced fluctuations of the NN exchange constant, result in qualitatively different behaviors of the dM/dB curve. The main consequence of the interaction with distant neighbors is a shift in the positions of the peaks and only small additional broadening, which is the same for all five peaks and can be described by introducing an effective temperature $T^* > T$, as given by Eq. (17). The two other mechanisms affect the dM/dB curve in a different way. Their main effect is the change in the amplitude of the peaks, with the amplitude being dependent on the number of the peak. Differences between the DM broadening and strain-induced broadening occurs mainly in the way they change the amplitude of the last two peaks in curve. This circumstance gives hope to better sort out the relative importance of each of these two mechanisms, and obtain more precise values of corresponding constants, D and dJ/dL. However, to do it one will need to carry out the measurements at very low temperatures and in strong (preferably static) applied magnetic fields. Also, at low temperatures it seems to be possible to extract information about the DM interaction by applying the magnetic field in different crystallographic directions, because the DM effect is slightly anisotropic. The experimental measurement of all the magnetization steps is not so easy as it involves the use of large pulsed magnetic fields that leads to (unknown) heating in the sample, which is probably not even in thermal equilibrium. The experimental results[15] are, therefore, not quite accurate enough to justify trying to make a detailed fit at this time, including all three mechanisms. We emphasize that all three mechanisms must be present, are all equally important in somewhat different ways, and the parameters are all known approximately from other experiments. The work of Larson, Haas, and Aggarwal[16] focused on the further neighbor interactions, to explain the peak widths in Cd/Mn compounds and consequently obtained a value of J_2 that is rather large and not consistent with other experimental determinations of J_2. These authors did not consider the other two broadening mechanisms that we have discussed here, but it is hard to understand why their value of J_2 was so large, as it was necessary to use this value to explain the uniform shift in all the peaks.

In conclusion, we have suggested that in diluted magnetic semiconductors there are fluctuations of exchange constant between neighboring magnetic ions. These fluctuations exist due to the bond-length mismatch in the solid alloy, which results in fluctuations of the distance between the ions. The theory of such fluctuations has been presented. We have shown that the fluctuations of the exchange constant provide a new mechanism for the broadening of the magnetization steps, which are observed in these compounds from the pairs of magnetic ions. This mechanism (the strain induced broadening) results in a qualitatively different behavior of the dM/dB curve from the mechanisms known before.

ACKNOWLEDGMENTS

We benefited from discussions with J. Cowen, Sir Roger Elliott, J. K. Furdyna, K. Hass, and J. Kossut. One of us (Y.G.R.) wishes to thank the Department of Physics and Astronomy of Michigan State University for their extremely warm hospitality extended to him during his visit when this work was done. This work was partially supported by NSF Grant No. DMR 9632182. We acknowledge J. K. Furdyna for sending us the detailed information and plots of the dependence of the exchange constant on Mn-Mn distance.

APPENDIX A: 2D NETWORK

We have added this appendix for two reasons. First, we want to show that the results similar to Eqs. (6)–(9) take place in the case when one has an alloy of diluted *bonds*. And second, we want to present the exact solutions for the lattice integrals, which can be obtained explicitly for a two-dimensional lattice.

We consider a 2D triangular net, the same as in Ref. 30. The bonds in this net can be of two types: A with probability $(1-x)$ and B with probability x. The natural bond lengths are L_A^0 and L_B^0, respectively, and the mean bond length is $L_e=(1-x)L_A^0+xL_B^0$. The dynamical matrix $\mathbf{D_{nm}}$ for this network is[30]

$$\mathbf{D_{lm}}=3\mathbf{I}, \quad \text{if } \mathbf{l}=\mathbf{m}, \tag{A1}$$

$$\mathbf{D_{lm}}=-\hat{\mathbf{r}}_{\mathbf{lm}}:\hat{\mathbf{r}}_{\mathbf{lm}}, \quad \text{if } \mathbf{l} \text{ is NN of } \mathbf{n}, \tag{A2}$$

where $\mathbf{I}$ is the unitary tensor, and the force constant, which is the common factor in these expressions, was omitted set equal to unity for simplicity.

Let us suppose, as we did in Sec. II, that we are interested in the properties of a B bond that connects neighboring sites $\mathbf{i}$ and $\mathbf{j}$, and that is surrounded by A bonds. These A bonds form again the cluster $\mathcal{V}_A$, and the cluster $\mathcal{V}_B$ consists in this case of only the B bond of interest. All the other bonds in the alloy are random. The average value of the length of this B bond, and its root-mean-square fluctuations, can be again expressed in terms of the Green function for the dynamical matrix (A1),(A2). Because we consider the case of diluted bonds, it turns out that it is more convenient to write the answers via sum over bonds, not over sites as in Sec. II. We denote the bonds using Greek letters and introduce the function $F_{\alpha\beta}$, which is analog of $a_{\mathbf{nm,i}}$,

$$F_{\alpha\beta}=\hat{\mathbf{r}}_{\mathbf{ij}}\cdot(\mathbf{G_{il}}+\mathbf{G_{jm}}-\mathbf{G_{im}}-\mathbf{G_{jl}})\cdot\hat{\mathbf{r}}_{\mathbf{lm}}. \tag{A3}$$

In Eq. (A3) it is assumed that α corresponds to the $\mathbf{ij}$ bond, and β corresponds to the $\mathbf{lm}$ bond. Then, it can be shown that the length of the B-bond L and its fluctuations are

$$\langle L\rangle=L_e+(L_A^0-L_B^0)\left[x\left(\sum_{\gamma\in\mathcal{V}_A}F_{\alpha\gamma}\right)-(1-x)F_{\alpha\alpha}\right], \tag{A4}$$

$$\langle(L-\langle L\rangle)^2\rangle=x(1-x)(L_A^0-L_B^0)^2\mathcal{R}_{\mathcal{V}}, \tag{A5}$$

$$\mathcal{R}_{\mathcal{V}}=\sum_{\beta\in\mathcal{V}}F_{\alpha\beta}^2, \tag{A6}$$

which are very similar to Eqs. (6)–(9).

For the triangular net under consideration there are some exact results concerning the function $F_{\alpha\beta}$ (see Ref. 30):

$$\sum_\beta F_{\alpha\beta}=0, \quad \sum_\beta F_{\alpha\beta}^2=F_{\alpha\alpha}=a^{**}=2/3, \tag{A7}$$

where the summation over β is without any restrictions. Unfortunately, there is no simple analytical results for the separate values of $F_{\alpha\beta}$. To calculate $F_{\alpha\beta}$ we can solve the equation for the Green function, $\Sigma_{\mathbf{n}}\mathbf{D_{mn}}\cdot\mathbf{G_{nl}}=\delta_{\mathbf{ml}}\mathbf{I}$, using the Fourier transform, and then obtain from Eq. (A3) the following expression:

$$F_{\alpha\beta}=\frac{S_0}{(2\pi)^2}\int d\mathbf{k}e^{i\mathbf{k}\cdot\mathbf{R}}(\hat{\mathbf{r}}_\alpha\cdot\mathbf{G}(\mathbf{k})\cdot\hat{\mathbf{r}}_\beta)4\sin(\tfrac{1}{2}L_e\mathbf{k}\cdot\hat{\mathbf{r}}_\alpha)\times\sin(\tfrac{1}{2}L_e\mathbf{k}\cdot\hat{\mathbf{r}}_\beta). \tag{A8}$$

Here vector $\mathbf{R}$ points from the middle of the α bond to the middle of the β bond, S_0 is the area of the Wigner-Zeitz cell, $S_0=(2/\sqrt{3})L_e^2$, and the integration over the wave vector $\mathbf{k}$ is restricted to the Brillouin zone. The tensor $\mathbf{G}(\mathbf{k})$ reads

$$G_{xx}=(\widetilde{A}+\widetilde{B})/\widetilde{D}, \quad G_{yy}=(\widetilde{A}-\widetilde{B})/\widetilde{D}, \tag{A9}$$

$$G_{xy}=G_{yx}=-\widetilde{C}/\widetilde{D} \tag{A10}$$

where

$$\widetilde{A}=3-\cos(k_xL_e)-2\cos(k_xL_e/2)\cos(\sqrt{3}k_yL_e/2), \tag{A11}$$

$$\widetilde{B}=\cos(k_xL_e)-\cos(k_xL_e/2)\cos(\sqrt{3}k_yL_e/2), \tag{A12}$$

$$\widetilde{C}=\sqrt{3}\sin(k_xL_e/2)\sin(\sqrt{3}k_yL_e/2). \tag{A13}$$

We have calculated the integrals (A8) numerically to find out how the factor $\mathcal{R}_{\mathcal{V}}$ (A6) changes with increasing the size of the cluster $\mathcal{V}$. The convergence of the integrals becomes poor with increasing of the distance $|\mathbf{R}|$ between the α and β bonds, and it is convenient to use the second relation (A7) which results in

$$\mathcal{R}_{\mathcal{V}}=a^{**}-\sum_{\beta\in\mathcal{V}}F_{\alpha\beta}^2. \tag{A14}$$

If there is no restriction, i.e., all the bonds, except the α bond, are taken at random, then the cluster $\mathcal{V}$ consists of the α bond only, and $\mathcal{R}_0=a^{**}(1-a^{**})=0.2222$. If the first shell of bonds around the α bond is filled with the A bonds (i.e., when the $\mathcal{V}_A$ cluster consists of the ten bonds attached to the α bond directly), we have $\mathcal{R}_1=0.1043$. When the A bonds occupy both the first and the second shell of bonds surrounding the α bond (i.e., when the $\mathcal{V}_A$ cluster consists of eighteen nearest bonds around the α bond), we have $\mathcal{R}_2=0.0653$.

It is important to understand what is the asymptotic behavior of $\mathcal{R}_n$ for large n. If two bonds, α and β, are separated by a macroscopic distance $|\mathbf{R}|\gg L_e$, the main contribution to the integral (A8) comes from the region of small wave vectors k. In this case we can perform the integration analytically. The result is

$$F_{\alpha\beta}=\frac{8}{9\pi}\frac{S_0}{R^2}(\hat{\mathbf{r}}_\alpha\hat{\mathbf{r}}_\beta)\left[(\hat{\mathbf{r}}_\alpha\hat{\mathbf{r}}_\beta)-2\frac{(\hat{\mathbf{r}}_\alpha\mathbf{R})(\hat{\mathbf{r}}_\beta\mathbf{R})}{R^2}\right]. \quad \text{(A15)}$$

Let us consider the case when the α bond (the B bond) is placed in the center of the circle of the macroscopic radius R_0. All the other bonds inside the circle are A bonds, and the bonds outside the circle are random. Substituting the above expression into Eq. (A6) and replacing the summation over bonds with the integration over their position, we obtain the asymptotic behavior of $\mathcal{R}_\mathcal{V}$:

$$\mathcal{R}_\mathcal{V}\rightarrow\frac{2^4}{3^3}\frac{S_0}{\pi R_0^2}. \quad \text{(A16)}$$

Such slow decay of the fluctuations of the bond length is a general result. It is because the propagations of the strain in the lattice over macroscopic distances is governed by long-wavelength acoustic phonons, and that is why $F_{\alpha\beta}$ for large distances between the bonds has the form of a dipole-dipole interaction. It is clear from this consideration that for a 3D lattice $\mathcal{R}_\mathcal{V}$ decays as R_0^{-3}.

*Permanent address: Institute of Semiconductor Physics, 252028, Kiev, Ukraine.
†Electronic address: thorpe@pa.msu.edu
‡Electronic address: mousseau@physcn.umontreal.ca

[1] J. C. Mikkelsen, Jr. and J. B. Boyce, Phys. Rev. Lett. **49**, 1412 (1982); Phys. Rev. B **28**, 7130 (1983); J. B. Boyce and J. C. Mikkelsen, Jr., *ibid.* **31**, 6903 (1985).
[2] A. Balzarotti, M. T. Czyzyk, A. Kisiel, N. Motta, M. Podgorny, and M. Zimnal-Starnawska, Phys. Rev. B **30**, 2295 (1984); A. Balzarotti, N. Motta, A. Kisiel, M. Zimnal-Starnawska, M. T. Czyzyk, and M. Podgorny, *ibid.* **31**, 7526 (1985).
[3] W.-F. Pong, R. A. Mayanovich, B. A. Bunker, J. K. Furdyna, and U. Debska, Phys. Rev. B **41**, 8440 (1990).
[4] L. Végard, Z. Phys. **5**, 17 (1921).
[5] Y. Cai and M. F. Thorpe, Phys. Rev. B **46**, 15 872 (1992); **46**, 15 879 (1992); N. Mousseau and M. F. Thorpe, *ibid.* **46**, 15 887 (1992).
[6] R. W. Wang, M. F. Thorpe, and N. Mousseau, Phys. Rev. B **52**, 17 191 (1995).
[7] J. G. Kirkwood, J. Chem. Phys. **7**, 506 (1939).
[8] P. N. Keating, Phys. Rev. **145**, 637 (1966).
[9] Different properties of DMS's are reviewed in book *Semimagnetic Semiconductors and Diluted Magnetic Semiconductors*, edited by M. Averous and M. Balkanski (Plenum, New York, 1991).
[10] B. E. Larson, K. C. Hass, H. Ehrenreich, and A. E. Carlson, Phys. Rev. B **37**, 4137 (1988).
[11] K. C. Hass, in Ref. 9, p. 59.
[12] J. Spalek, A. Lewicki, Z. Tarnawski, J. K. Furdyna, R. R. Galazka, and Z. Obuszko, Phys. Rev. B **33**, 3407 (1986).
[13] A. Bruno and J. P. Lascaray, Phys. Rev. B **38**, 9168 (1988).
[14] Y. Shapira, in Ref. 9, p. 121.
[15] S. Foner, Y. Shapira, D. Heiman, P. Becla, R. Kershaw, K. Dwight, and A. Wold, Phys. Rev. B **39**, 11 793 (1989).
[16] B. E. Larson, K. C. Hass, and R. L. Aggarwal, Phys. Rev. B **33**, 1789 (1986).
[17] Y. Shapira, S. Foner, D. Heiman, P. A. Wolff, and C. R. McIntyre, Solid State Commun. **71**, 355 (1989).
[18] B. E. Larson and H. Ehrenreich, Phys. Rev. B **39**, 1747 (1989).
[19] N. Samarth and J. K. Furdyna, Solid State Commun. **65**, 801 (1988).
[20] W. H. Press, B. P. Flannery, S. A. Teukolsky, and W. T Vetterling, *Numerical Recipes* (Cambridge University Press, Cambridge 1986).
[21] R. E. Behringer, J. Chem. Phys. **29**, 537 (1958).
[22] N. Mousseau and M. F. Thorpe, Phys. Rev. B **48**, 5172 (1993).
[23] A. Twardowski, H. J. M. Swagten, W. J. M. de Jonge, and M. Demianiuk, Phys. Rev. B **36**, 7013 (1987).
[24] S. Nagata, R. R. Galazka, D. P. Mullin, H. Akbarzadeh, G. D. Khattak, J. K. Furdyna, and P. H. Keesom, Phys. Rev. B **22**, 3331 (1980).
[25] T. M. Giebultowicz, J. J. Rhyne, and J. K. Furdyna, J. Appl. Phys. **61**(8), 3537 (1987); T. M. Giebultowicz, J. J. Rhyne, W. Y. Ching, D. L. Huber, J. K. Furdyna, B. Lebech, and R. R. Galazka, Phys. Rev. B **39**, 6857 (1989); T. M. Giebultowicz, J. J. Rhyne, J. K. Furdyna, and P. Klosowski, J. Appl. Phys. **67**,(9) **67**, 5096 (1990).
[26] D. Scalbert, Mater. Sci. Forum **182–184**, 451 (1995).
[27] D. R. Yoder-Short, U. Debska, and J. K. Furdyna, J. Appl. Phys. **58**(11), 4056 (1985).
[28] J. A. van Vechten and J. C. Phillips, Phys. Rev. B **2**, 2160 (1970).
[29] S.-H. Wei and A. Zunger, Phys. Rev. Lett. **56**, 2391 (1986); Phys. Rev. B **35**, 2340 (1987).
[30] E. J. Garboczi and M. F. Thorpe, Phys. Rev. B **32**, 7276 (1985); M. F. Thorpe and E. J. Garbozci, *ibid.* **42**, 8405 (1990).